Molecular Dynamics Simulation of the Cyclic Decapeptide Antibiotic, Gramicidin S, in Dimethyl Sulfoxide Solution

Dan Mihailescu[†,‡] and Jeremy C. Smith*[,†,§]

SBPM, DBCM, Commissariat à L'Energie Atomique, CEA-Saclay, 911191, Gif-sur-Yvette, France, Faculty of Biology, University of Bucharest, Spl. Independentei, 91-95, 76201, Bucharest, Romania, and Lehrstuhl für Biocomputing, IWR, Universität Heidelberg, D-69120, Heidelberg, Germany

Received: September 10, 1998

We report on a 5 ns molecular dynamics simulation of the decapeptide antibiotic, gramicidin S (*cyclo*-(Leu-DPhe-Pro-Val-Orn)$_2$) in dimethyl sulfoxide solution. Throughout the simulation the backbone ring maintains an antiparallel β-pleated sheet conformation with two type II′ β-turns. The backbone dihedrals are relatively inflexible and do not undergo any conformational transitions. The simulation reproduces the Φ and Ψ angles derived from nuclear magnetic resonance spectroscopy to within 18° standard deviation on average. Correlations between the backbone dihedral angles are found. The side chain dihedrals are much more flexible, and the multiple conformational states of these are classified using a clustering technique. Side chain hydrogen-bonding involving the ornithine and phenylalanine residues is analyzed and discussed in the context of previous work.

Introduction

Gramicidin S (GS) is a cyclic peptide antibiotic with the sequence *cyclo*-(Leu-D-Phe-Pro-Val-Orn)$_2$. It was first isolated in 1944 from *Bacillus brevis.*[1] It exhibits a broad spectrum of antibiotic behavior, acting on both gram-positive and gram-negative bacteria.[2] Unfortunately, GS also has the capacity to affect virtually all other types of cell membranes and exhibits marked hemolytic activity, and this has hindered its therapeutic use.[3] Since the isolation of GS, more than 200 analogues of it have been synthesized with the goals of better defining its structure−activity relationships and extending the activity of the compound to produce a more potent and more specific antibiotic.

Drug design initiatives should benefit from a physical chemical understanding of the mechanism of action of GS at the molecular level. Although the details of GS action are still unknown, it has been shown that it interacts very strongly with natural and model lipid membranes and strongly degrades their permeability properties.[4−6] Moreover, the high activity of *enantio*-GS argues against the existence of a specific macromolecular receptor.[7] Studies of the interaction of GS with model lipid membranes suggest that it interacts primarily with the headgroup and interfacial polar/apolar regions of the membranes.[8−10]

The conformational properties of GS can be expected to play a major role in its activity, and this is a major reason that work has been undertaken to gain an understanding of its structure and flexibility in different environments. Further impetus to such studies is provided by the relative simplicity of the GS primary sequence, which is C_2 symmetric. Early crystallographic work on a GS−urea complex revealed an antiparallel β-pleated sheet structure with two type II′ β-turns.[11] Four transannular symmetric hydrogen bonds between Leu and Val residues, stabilizing the secondary structure, were seen. A fifth hydrogen bond was also present in the crystal structure, between a N_δ of Orn and the CO group of D-Phe, and was found to break the C_2 intramolecular symmetry in the primary sequence.

Various nuclear magnetic resonance (NMR) methods have been applied to obtain structural information on GS in solution.[12−20] These studies, together with circular dichroism (CD) and infrared results,[21−23] confirmed the presence of the β-sheet and indicated that the time-averaged solution structure is indeed C_2 symmetric. Magnetization transfer experiments indicated that the D-Phe-Pro sequences again form type II′ β-turns.[13,17] In most of the conformational studies, two solvents were used: methanol and dimethyl sulfoxide (DMSO). The conformation of the backbone ring, as defined by the dihedral angles Φ and Ψ, was found to be the same to within experimental error in both these solvents.[12,13,20] In contrast, conformational properties of the side chains were found to be solvent-dependent.

Structure−function studies led to the proposal of a "sidedness hypothesis".[24] The two main points of this are as follows. (i) The two type II′ β-turns at the D-Phe-Pro segments play a role in the antimicrobial activity. If the peptide cannot form the β-turn conformations, the antimicrobial activity is markedly reduced. (ii) The molecule must be amphipathic, with the two ornithine side chains on one side of the average molecular plane and the hydrophobic side chains on the other. NMR and CD studies on analogues with Orn residues replaced indicated that they are necessary for activity.[25−27]

In early conformational calculations, the symmetry of the primary structure of GS was assumed to extend to three dimensions.[21,28] This hypothesis was also applied in work on the conformational analysis of the molecule using empirical molecular mechanics energy functions.[29−32] Although these calculations provided valuable insight into the conformational properties of GS, more recent, molecular dynamics (MD) techniques can be expected to furnish additional useful information for several reasons. Among these is the fact that, rather

† SBPM, DBCM, Commissariat à L'Energie Atomique.
‡ University of Bucharest.
§ IWR, Universität Heidelberg.

10.1021/jp983674t CCC: $18.00
Published on Web 02/17/1999

than reduction of the scope of calculations by using the arbitrary assumption of C_2 symmetry for all configurations, it should be more accurate to remove this condition and to examine and average over nonsymmetric configurations. Furthermore, MD allows the convenient explicit inclusion of solvent molecules.

Among the 20−30 NMR studies on GS, three are of particular interest for the present work.[18−20] First, Krauss and Chan revealed that in methanol the Orn chain of GS is involved in an H-bond of a type similar to that in the crystal structure.[18] Second, Jones et al. published a comprehensive NMR study on the χ_1 rotamers of GS.[19] Finally, in recent work, Xu et al. reported on structural features of GS obtained from an intensity-restrained global structural optimization of NMR NOESY data on GS dissolved in DMSO.[20]

The existence of the NMR data provides further motivation for the application of MD techniques to examine the structure and dynamics of GS. Here, we report results of a 5 ns MD simulation of GS in DMSO solution. The structural parameters obtained are compared with those derived from the NMR work in refs 18−20. We find that the antiparallel β-sheet and turns are maintained throughout the simulation. The backbone ring structure is relatively rigid, with Φ and Ψ angles mostly close to experimental values. In contrast, the side chains undergo many conformational transitions, and these are grouped here into clusters. Finally, we examine hydrogen-bonding and other structural properties of the ornithine side chains. The calculations, using a system that is experimentally relatively well-defined, represent a first step toward the obtention of an accurate simulation model of GS−membrane interaction.

Methods

The model system is GS in a box of DMSO replicated with periodic boundary conditions. DMSO was chosen as the solvent to enable comparison with the most detailed available NMR data. The simulation box included one molecule of GS and 193 molecules of DMSO. The program used was CHARMM, version 24.[33] The all-atom CHARMM force field version 22.0[34] was used for all peptide residues except Orn, for which the force field topology and parameters were derived using Lys from ref 34 as a model, thus taking advantage of the close relationship in the chemical structure of these two residues; the Lys residue has an extra CH_2 group. A force field for DMSO[35] has been applied in MD simulation of Leu-enkephalin in DMSO.[36] For the present work, the parameters from ref 35 were adapted for the CHARMM potential function. The Orn and DMSO parameters used are listed in the Appendix.

The cutoff for the nonbonded interactions was 13 Å. The side of the simulation box was 29.5 Å. The SHAKE algorithm was applied in order to constrain bonds, thus allowing the use of a time step of 2 fs. The electrostatic interactions were smoothed using the SWITCH method,[33] which involves multiplication by a cubic function, in this case between 12 and 13 Å.

The starting structure was chosen to include an idealized C_2-symmetric cyclic backbone geometry. The evolution of this structure toward or away from the experimental NMR results was then examined by simulation. The starting structure for one-half of the GS molecule was obtained from the standard CHARMM internal coordinate table. C_2 symmetry was applied to generate the other half, and the two halves were linked with peptide bonds. The energy was minimized with $\epsilon_r = 45$ (the relative dielectric constant for DMSO), maintaining the C_2 symmetry condition on the system. For subsequent calculations no symmetry conditions were applied. The energy-minimized GS was placed in a box of DMSO having the experimental density of the pure solvent, 1.1014 g/cm^3. The GS molecule was fixed and the solvent energy minimized to a root-mean-square (rms) energy gradient that is $<10^{-4}$ kcal mol^{-1} Å^{-1}. After this step, all atoms were allowed to move and the energy of the whole system was minimized to the same gradient accuracy. The system was heated with Verlet MD up to 300 K and equilibrated with velocity rescaling at this temperature. For small peptides, the equilibration is a key phase; an unequilibrated system has been found to give rise to "unnatural transitions".[36] The equilibration was therefore pursued to 2 ns of simulation time. Subsequently, the production dynamics was run for 5 ns in the microcanonical ensemble. The coordinates and velocities were saved every 100 steps. The temperature was 300 ± 7 K. The calculations took 200 central processing unit hours on a Sun UltraSPARC 170 MHz computer.

Results

Backbone Conformation. The backbone of GS and the Orn side chains are shown in a dynamical snapshot in Figure 1. The peptide backbone was found to maintain an antiparallel β-sheet conformation throughout the 5 ns simulation. The general shape of the backbone ring was elliptical. The long axis of the ellipse can be conveniently defined as the vector between the C_α atoms of Pro-3 and Pro-8 and the short axis by the vector between the C_α atoms of Leu-1 and Val-4. The time dependence of the two axes lengths is presented in Figure 2. Both lengths remain quite constant, fluctuating by 2−4%.

The C_α atoms of the GS backbone lie approximately in a plane, which can be described by the equation $lx + my + nz = p$. If **n** is the vector normal directed through the plane from the origin of the Cartesian axes (x, y, z), then l, m, and n are the axis projections of **n**. p is the projection of **r** on **n**, where **r** is the position vector of a point on the plane relative to the origin of the axes. Time series of l, m, n, and p are presented in Figure 3. The normal to the backbone atoms plane varies little in the z direction ($z = -0.96 \pm 0.01$), and the distance between the origin of the axes and the plane is also stable ($p = 1.32 \pm 0.10$). The normal to the ellipse plane varies more but lies on the surface of a cone having the z-axis as the symmetry axis.

Time series for the distances of the C_α atoms to the ellipse plane are shown in Figure 4. The α-carbons of Phe, Val, and Orn lie very close to the plane, and the other two residues are at distances of <2 Å. All the C_α atoms, except those of Pro, show slow variation of their distances to the plane, on the nanosecond time scale.

The average main-chain dihedral angles are presented in Figure 5 together with their rms fluctuations and the corresponding NMR values. The simulation is close to experiment for most of the dihedrals, the average standard deviation from experiment being 18°. Trial simulations indicated that the Φ, Ψ fluctuations obtained depend on the equilibration time. In simulations performed with equilibration times of <100 ps, the rms fluctuations of the Φ and Ψ angles were between 20° and 50°. In the final simulation, which was equilibrated for 2 ns with 5 ns production, the rms fluctuations are much smaller. The β-turn is of type II′ throughout the simulation. The fluctuations of the backbone dihedrals of residues involved in the β-turns (D-Phe-2, Pro-3, D-Phe-7, and Pro 8) are on average lower than those of the other residues.

No conformational transitions were found for any of the backbone dihedrals. Figure 6 presents some backbone dihedral

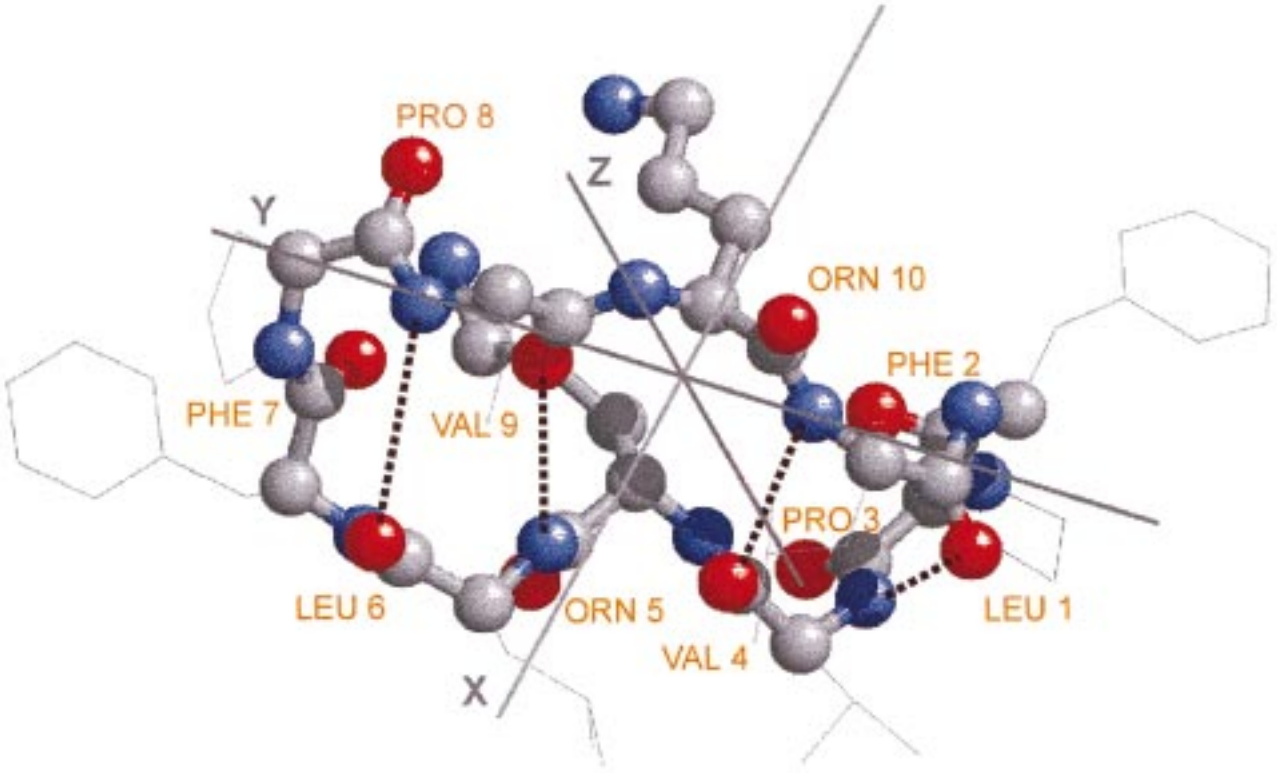

Figure 1. Snapshot of GS molecule in the MD simulation. The backbone heavy atoms and the Orn side chain heavy atoms are in the ball-and-stick representation. The hydrogen bonds are represented as dotted lines between the donor and acceptor residues Leu and Val. The orientation of the Cartesian frame coordinate axes is also shown. The DMSO molecules are omitted for clarity. The plot was obtained using the "RASMOL" software.

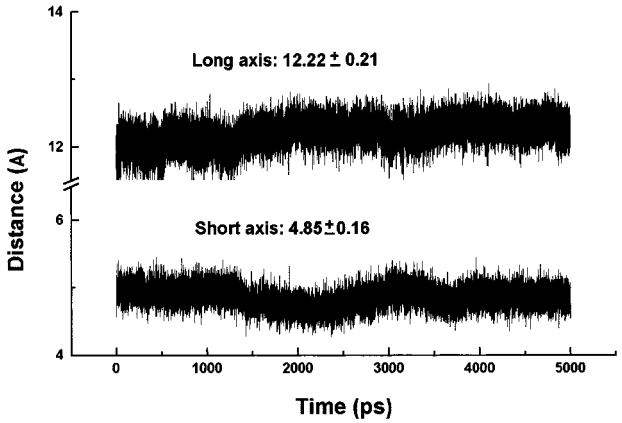

Figure 2. Time series of the axes of the GS ring ellipse.

angle time series. An example of a time series for a dihedral with small fluctuations is shown in Figure 6c; only fast oscillations are seen. This can be contrasted with dihedrals with larger fluctuations, such as that in Figure 6f, in which slow, nanosecond time scale variations are superposed on the fast oscillations.

The overall picture that arises from the above analysis is that the backbone remains in one potential energy well and is relatively rigid. This is consistent with the conclusions from several NMR analyses of GS in solution.[13,17−19] One possibile consequence of this is that the rigidity of the ring may lead to correlation between dynamical perturbations among the torsional angles. To examine this further, equal-time correlations between the backbone dihedrals were analyzed by constructing a matrix of plots (Figure 7). In each individual plot a $\Delta\Phi(t)$ or $\Delta\Psi(t)$ is given as a function of another $\Delta\Phi(t)$ or $\Delta\Psi(t)$, where $\Delta\Phi(t) = \Phi(t) - \bar{\Phi}$ and $\Delta\Psi(t) = \Psi(t) - \bar{\Psi}$. If the fitted line is horizontal, no correlation exists between the corresponding dihedrals. A positive slope indicates that the angles are positively correlated, and a negative slope indicates they are anticorrelated. The plots in rounded boxes in Figure 7 demonstrate a significant anticorrelation between $\Delta\Phi_i$ and $\Delta\Psi_{i-1}$. A similar, $\Delta\Phi_i/\Delta\Psi_{i-1}$ anticorrelation has previously been shown in protein backbone dihedral transitions.[36,37] However, in the present case anticorrelation is observed in a system that undergoes no transitions, i.e., within a single potential well. For Leu-6, a succession of correlation−anticorrelations (positive and negative slopes) can be observed in neighboring residues (rectangular boxes). Similar behavior is observed for Val-9. This observation may indicate the existence of a wave phenomenon in some parts of the GS ring. However, the examination of appropriate time correlation functions (not shown) indicated that the simulation statistics were insufficient for further characterization of this effect.

Side Chain Rotamers. Wheras the backbone of GS was found to populate only one minimum in the simulation, the side chains were found to exhibit considerable conformational flexibility, with the χ angles sampling one, two, or occasionally, three or more conformations. Table 1 presents the results of a cluster analysis of the χ_1 angles using the algorithm presented in ref 38. This algorithm, based on a self-organising neural net, optimizes cluster assignment such that no member of a cluster is more than a specified distance (cutoff radius) from the cluster center. For each pattern of cluster distribution, the standard deviation (Euclidean distance) from the cluster center and the cluster members are calculated. The data presented in Table 1 were obtained using a cutoff radius of 60°. This value was found suitable for sorting all the conformers, and the resulting standard deviations are in the same range as the MD fluctuations: $<13°$.

The simulation results for the conformations of the χ_1 angles can be compared with NMR results in refs 19 and 20. There

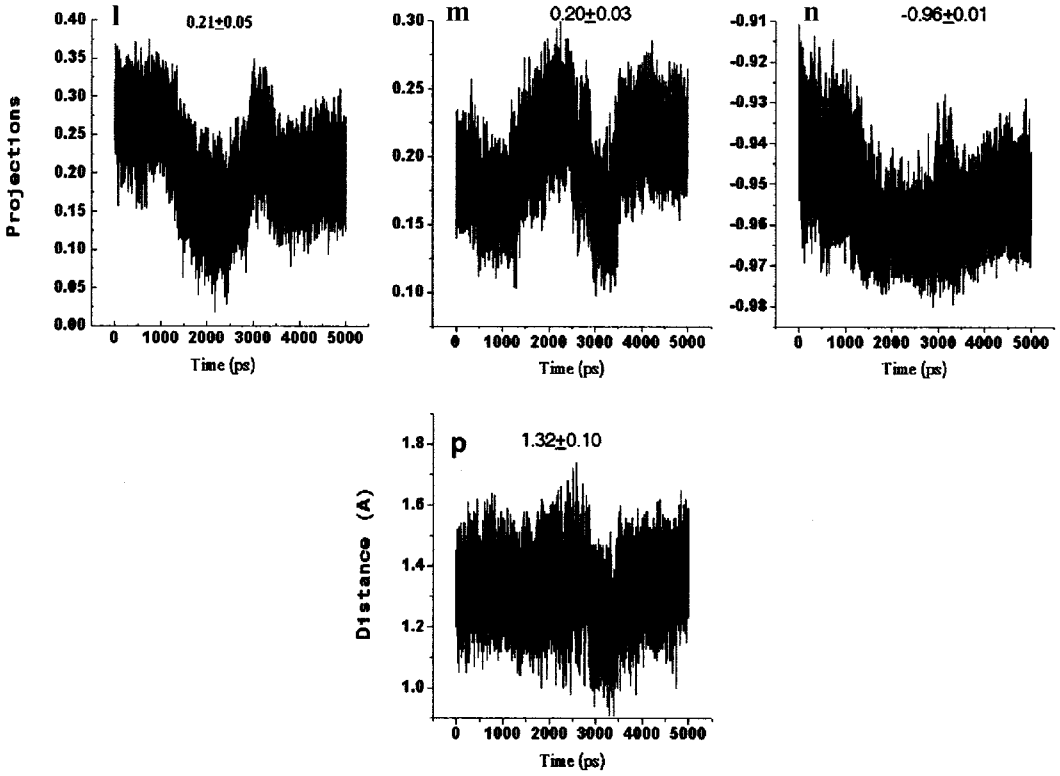

Figure 3. Time series of *l*, *m*, *n*, and *p* parameters that define the GS backbone plane.

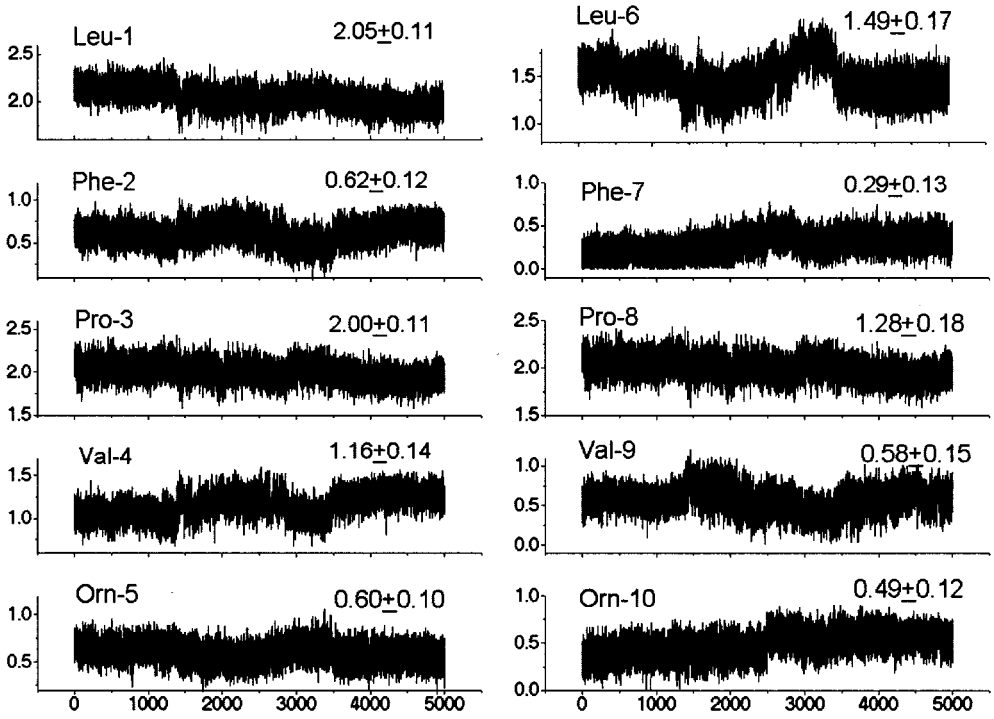

Figure 4. Time series for the distances of the α-C of the amino acids to the elliptical plane. The average distances and standard deviations are also indicated. All the distances are in angstroms.

are considerable differences in the results obtained for the average χ_1 values in the two NMR studies. These differences may arise from several sources, including the type of NMR signal examined, the refinement method, and the solvent. In particular, however, in ref 20 only the average values were reported for the side chain dihedrals. In systems fluctuating between several minima, this is of limited value. Table 1 shows that most of the conformers populated in the NMR analysis of ref 19 are also populated in the simulation, although to different degrees. χ_2, χ_3, and χ_4 rotamer data are listed in Table 2. Multiple conformations are apparent for most of these side chain dihedrals.

The side chain torsions, both intra- and interresidue, are likely to be interdependent. Therefore, the possibility exists that the entire side chain conformational space can be grouped into a relatively small number of classes. To examine this further, the cluster analysis was carried out on the whole set of χ angle conformations. By use of a cutoff radius of 75°, five confor-

TABLE 1: Cluster Analysis of χ_1 Rotamer Populations[a]

residue	cluster	no. of members	R (deg)	χ_1 sim ± SD (deg)	χ_1 sim average ± rms (deg)	χ_1 average from ref 19 NMR (deg)	χ_1 from ref 20 NMR (deg)	χ_1 relative populations[19] and in MD 180°	−60°	+60°
Leu-1	1	24737	40	−58 ± 9	−57 ± 9	54 ± 5	−20...−60[b]	0.4	0.4	0.1
	2	263	37	−123 ± 2			82			
Leu-6	1	25000	36	−59 ± 8	−58 ± 7			**0**	**~1**	**0**
Phe-2	1	25000	37	79 ± 8	82 ± 8	114 ± 11	172	0.7	0	0.2
Phe-7	1	25000	26	173 ± 7	171 ± 7			**0.5**	**0**	**0.5**
Val-4	1	25000	42	−165 ± 8	−164 ± 8.	90 ± 9	178	0.5	0.4 (0°)	0.4 (0°)
Val-9	1	21582	45	−70 ± 10	−107 ± 51					
	2	3418	52	177 ± 9				**0.6**	**0.4**	**0**
Orn-5	1	25000	47	168 ± 9	169 ± 10	6 ± 1	−55 (−63 and 166)	0.2	0.6	0.1
Orn-10	1	24731	59	−61 ± 10	−62 ± 10			**0.5**	**0.5**	**0**
	2	269	56	−176 ± 13						

[a] The columns list the residue symbol, the cluster index number, the number of members in the cluster (the total number of configurations analyzed in the simulation was 25 000), the radius of the cluster (R), the cluster center ± the standard deviation (SD), the simulation average χ_1 ± the root-mean-square (rms) fluctuation from the average, χ_1 averages calculated from ref 19, the values of χ_1 reported in ref 20, the relative populations for conformation for 180°, −60°, +60° in ref 19 and in the present simulation. Two conformers, 180° and 0°, were found for Val in ref 19. [b] The −20° to −60° Leu conformation was provided by R. Rama Krishna (personal communication).

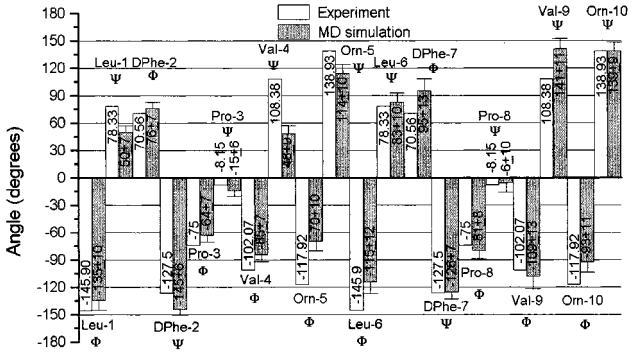

Figure 5. Averages and fluctuations of the main-chain dihedrals (Φ and Ψ) of GS obtained in this simulation study and by NMR.[20] In the NMR study the molecule was assumed to be C_2 symmetric. In ref 20, the experimental data were presented without the corresponding errors and every angle was reported with two digits below the decimal point.

mational clusters, approximately equipopulated, were found. These are listed in Table 3.

Hydrogen Bonds. Experiments using X-ray diffraction,[11] CD,[39] and NMR[12] have provided evidence for the existence of two pairs of backbone hydrogen bonds, O-Leu-1···NH-Val-4, O-Leu-6···NH-Val-9, O-Val-4···NH-Leu-1, and O-Val-9···NH-Leu-6. During the MD simulation the distances O···N of Leu-1···Val-4 and Leu-6···Val-9 were 3.66 ± 0.24 and 4.15 ± 0.32 Å. The distances N···O of Leu-1···Val-4 and Leu-6···Val-9 were 3.27 ± 0.24 and 3.00 ± 0.16 Å. Therefore, the two pairs of Leu-Val hydrogen bonds found experimentally are also found in the present simulation. They are illustrated in Figure 1.

The side chain hydrogen bonding has been debated in the literature.[11,18,31] In particular, the question arises as to whether there is an H-bond between N_δ of Orn and CO of Phe, and if so, whether this is on one half or both halves of the molecule. Furthermore, if the H-bond does exist, it may be in principle of order $i \rightarrow i + 2$ or $i \rightarrow i - 3$, where i is the residue number. In previous theoretical work, energy minimization in a vacuum led to two symmetric side chain H-bonds, between N_δ of Orn and the CO group of the D-Phe preceding the Orn in the sequence, i.e., $i \rightarrow i - 3$.[30,31] In contrast, the X-ray structure contained only one side chain H-bond, and that was between the Orn side chain and the D-Phe that follows it (5 →

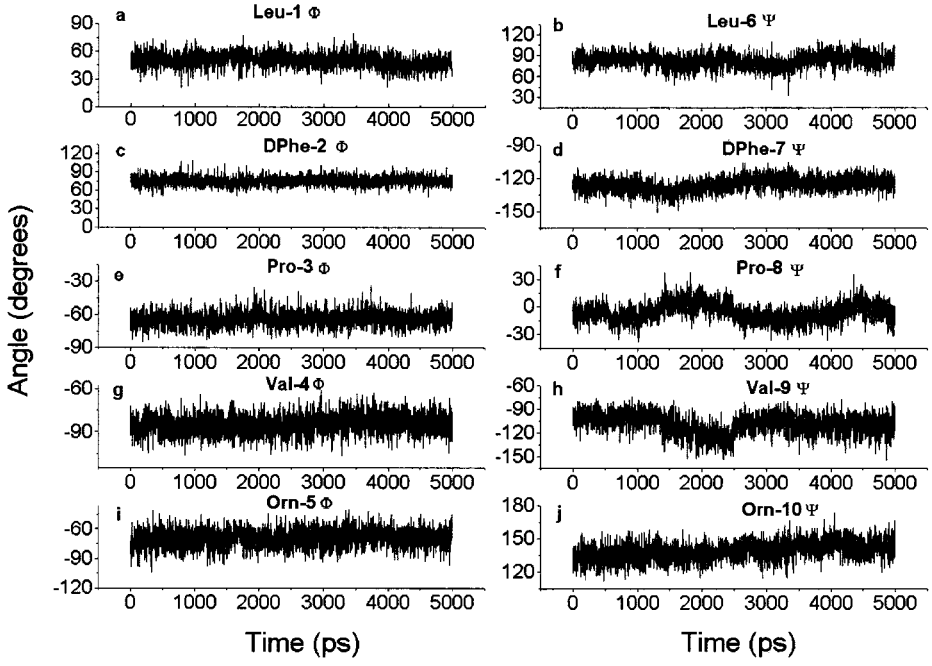

Figure 6. Time series for Φ and Ψ angles.

TABLE 2: Rotamer Conformations of χ_2, χ_3, and χ_4 Side Chains[a]

residue	cluster	no. of members	R (deg)	$\chi \pm$ SD MD (deg)
				χ_2
Leu-1	1	24115	38	166 ± 8
	2	885	44	83 ± 12
Leu-6	1	25000	38	174 ± 9
Phe-3	1	24909	41	-118 ± 9
	2	91	47	164 ± 17
Phe-8	1	25000	44	95 ± 11
Val-4	1	8852	59	179 ± 16
	2	8301	59	-63 ± 16
	3	7847	53	73 ± 12
Val-9	1	13718	59	177 ± 14
	2	6942	59	-56 ± 14
	3	4340	54	54 ± 9
Orn-5	1	24348	32	-104 ± 9
	2	652	54	-153 ± 20
Orn-10	1	25000	60	-177 ± 9
				χ_3
Leu	1	6086	59	-59 ± 13
	2	9064	59	-178 ± 13
	3	9850	57	61 ± 13
Leu	1	7982	58	61 ± 14
	2	9181	60	-179 ± 14
	3	7837	54	-70 ± 10
Val	1	8446	54	58 ± 9
	2	8939	50	-65 ± 10
	3	7615	53	-173 ± 13
Val	1	7695	58	-62 ± 14
	2	8005	60	178 ± 13
	3	9300	55	69 ± 9
Orn	1	2778	39	-175 ± 11
	2	21916	39	-73 ± 8
	3	306	31	62 ± 13
Orn	1	3037	50	165 ± 14
	2	21032	40	64 ± 10
	5	931	56	-62 ± 16
				χ_4
Leu	1	8801	60	-61 ± 14
	2	8311	59	179 ± 14
	3	7888	54	70 ± 9
Leu	1	7823	48	73 ± 10
	2	9181	53	-72 ± 10
	3	7996	54	-179 ± 15
Orn	1	10234	34	160 ± 14
	2	5299	34	93 ± 13
	3	4799	58	57 ± 15
	4	2481	31	-123 ± 15
	5	2187	58	-60 ± 21
Orn	1	11062	35	-170 ± 13
	2	2382	35	-100 ± 15
	3	3696	58	-60 ± 15
	4	4635	58	59 ± 13
	5	3225	31	94 ± 14

[a] The columns are the same as the first four columns of Table 1.

7 or 10 → 2), i.e., $i \rightarrow i + 2$.[11] The difference between the energy-minimized structure and the conclusions from the X-ray experiment was rationalized by Nemethy and Scheraga who proposed a revised structure (in another potential energy minimum) that indeed permitted the hydrogen bond to adopt the X-ray structure.[32]

An NMR investigation of GS in various solvents was interpreted in terms of strongly solvent-dependent side chain H-bonding.[18] In methanol, the H-bonding is of the $i \rightarrow i + 2$ type.[18] In DMSO the side chain H-bonding situation is unclear. The NMR data in DMSO from ref 20 were interpreteted as being compatible with the existence of two distinct conformers for the ornithine side chain, forming hydrogen bonds with Phe in both the $i \rightarrow i + 2$ and $i \rightarrow i - 3$ senses. This involved two equiprobable Orn χ_1 conformations at $-63°$ and $166°$. These

TABLE 3: Clustering of Conformational Distribution of GS

cluster	no. of members	SD	R (deg)	residue	χ_1	χ_2	χ_3	χ_4
1	4175	49	74	Leu	−58	164	140	162
				Phe	79	−117		
				Val	−165	158	52	
				Orn	169	−92	−48	102
				Leu	−59	174	35	−144
				Phe	174	96		
				Val	−87	104	−84	
				Orn	−61	−178	63	−128
2	4478	50	69	Leu	−58	161	−176	−159
				Phe	80	−118		
				Val	−164	−28	−107	
				Orn	168	−92	−53	148
				Leu	−59	174	161	168
				Phe	174	95		
				Val	−91	−1	16	
				Orn	−62	−177	68	−127
3	5049	51	71	Leu	−59	162	−117	32
				Phe	78	−117		
				Val	−165	74	−65	
				Orn	167	−96	−59	165
				Leu	−60	174	−45	−60
				Phe	174	94		
				Val	−83	−55	143	
				Orn	−67	−178	64	150
4	5261	50	72	Leu	−58	165	66	176
				Phe	78	−118		
				Val	−165	−10	113	
				Orn	168	−98	−58	180
				Leu	−59	175	174	−62
				Phe	173	96		
				Val	−81	120	66	
				Orn	−61	−177	89	128
5	6037	50.1	72.8	Leu	−59	165	35	−55
				Phe	78	−118		
				Val	−166	−152	38	
				Orn	168	−95	−77	160
				Leu	−59	174	178	62
				Phe	173	96		
				Val	−81	−177	−93	
				Orn	−60	−177	70	144

conformations were both found in the simulation, at $-61°$ and $-176°$. For the χ_2 angle of Orn, Xu et al. fitted their data using again two conformers of equal probability, at $-170°$ and $72°$. As can be seen from Table 2, one of the Orn residues in the simulation does sample two conformers, one of which is close to one of the conformers in ref 20, whereas the other is not. The conformation at $72°$ considered by Xu et al. was not sampled in the simulation in either Orn residue.

By inspection of the average MD values in Table 4, only Orn-5 $N_\delta \cdots O$ D-Phe-7 might correspond to a hydrogen bond, this being very weak. However, the time series for this $N_\delta \cdots O$ distance, shown in Figure 8a, provides evidence for a small subpopulation at <3.5 Å, corresponding to a stronger H-bond. The relative population of the Orn-5 chain involved in the stronger H-bond is 0.11 of the total, corresponding to a difference in free energy between the "bound" and "unbound" states of 5.5 kJ/mol. This value can be compared with the value for GS in methanol derived from NMR of 9.6 ± 1.7 kJ/mol.[19] The lowest energy states were the same in both MD and NMR: unbound. The quantitative difference in the free energies obtained may arise from several sources. There are likely to be incomplete sampling and other inaccuracies in the MD simulation. However, there are also different definitions for the two states (acceptor−donor distance in MD and chemical shifts in the NMR), and there might also be a solvent effect, in which in DMSO the energy difference between the two states would be lower than in methanol.

TABLE 4: Distance between N_δ Atom of Orn Residue and O Atom of D-Phe Obtained via Different Methods[a]

method	distance, N_δ 5 Orn to 2 O D-Phe (Å)	distance, N_δ 10 Orn to 2 O D-Phe (Å)	distance, N_δ 5 Orn to 7 O Phe (Å)	distance, N_δ 10 Orn to 7 O Phe (Å)
present work	6.45 ± 0.48	5.38 ± 0.44	4.45 ± 0.59	8.53 ± 0.52
vacuum minimization[32]	2.92		2.92	
X-ray crystallography[11]	2.82		2.82	

[a] The X-ray experiment reported the value for one of the two distances.[11]

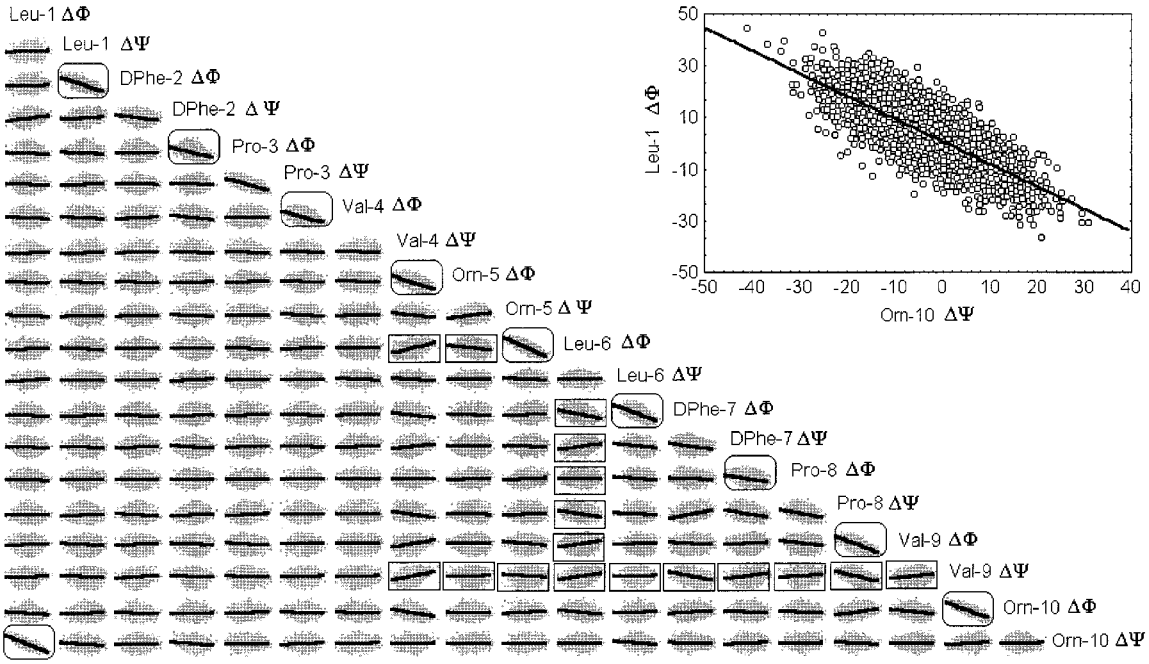

Figure 7. Matrix representation of $\Delta\Phi_i = f(\Delta\Psi_j)$ and $\Delta\Psi_i = f(\Delta\Phi_j)$ for all dihedral angle pairs except $i \neq j$. In the top right half of the figure is shown an enlarged plot of one of the pair distributions. The angles corresponding to every row and column of the matrix are given at the head of the columns. The best-fit straight line to every distribution is also represented.

The simulation also provided evidence for significant population of a specific ornithine solvation structure. This was seen from $t \approx 200-2100$ ps, during which time the distance between the two Orn N_δ groups was relatively short (~4 Å; see Figure 8b). An illustration of the structure is given in Figure 9, in which the positions of the two Orn chains, the D-Phe-7 chain involved in the H-bond with Orn-5, and the two closest DMSO molecules are presented. A roughly symmetric structure is formed, with the N_δ atom of Orn-5 in the center and the oxygen atoms of D-Phe-7 and of the two DMSO molecules in the corners.

Finally, we examine the orientation of the two Orn residues with respect to the backbone elliptical plane. Time series of the relevant *z*-projections are shown in parts c and d of Figure 8. The direction of the Orn chain involved in the H-bond with D-Phe is almost all the time perpendicular to the GS backbone plane, the *z*-projection being close to −1. The other Orn residue, which is not involved in an H-bond, is much more flexible but stays on the same side of the molecular plane as the first Orn, the *z* projection remaining negative (Figure 9). Thus, the amphipathic character of the molecule, essential to the sidedness hypothesis, is preserved.

Conclusions

The present simulation results provide a dynamical model for GS in DMSO, which is of interest for essentially two reasons: as a simple model antiparallel β-structure and as a starting point for the obtention of a reliable simulation model of key events in the antibiotic activity of GS.

GS provides a convenient system with which to examine structural and dynamical properties of the fundamental protein β-elements. Several NMR studies indicate that GS possesses a relatively rigid backbone but strongly fluctuating side chains.[12−19] This was also found in the present study, and the agreement between experiment and simulation for the backbone Φ and Ψ angles gives confidence for the extension of this approach to other solvents and more complex environments.

Comparison with experimental results for the side chain conformations is more difficult. This is due in part to the limitations in the dynamical models used for refining the NMR data. It is hoped that in the future more direct combination of simulation and NMR measurements might provide more reliable models for NMR analysis. One possibiity is that weighted clusters such as those detailed in Table 3 might be used to constrain NMR refinement. However, as ever, there will also be limitations in the simulation work, due to imprecision in the potential function, approximations in the simulation methodology, and the limited production time, 5 ns in the present case. The effect of limited simulation time is illustrated in the present work, since several of the time series presented exhibit dynamical phenomena with characteristic relaxation times of the order of the simulation length, which will consequently be undersampled. Moreover, C_2 symmetry of the time-averaged structure is not yet achieved; this would be expected for a converged simulation.

While bearing the above limitations in mind, the extension of the present work to the examination of GS analogue structures in pure solvents should be relatively straightforward. The antibiotic target of GS is the membrane lipid bilayer, which is a more complicated and expensive system to model. However, arguably, sufficient information exists on the GS−headgroup

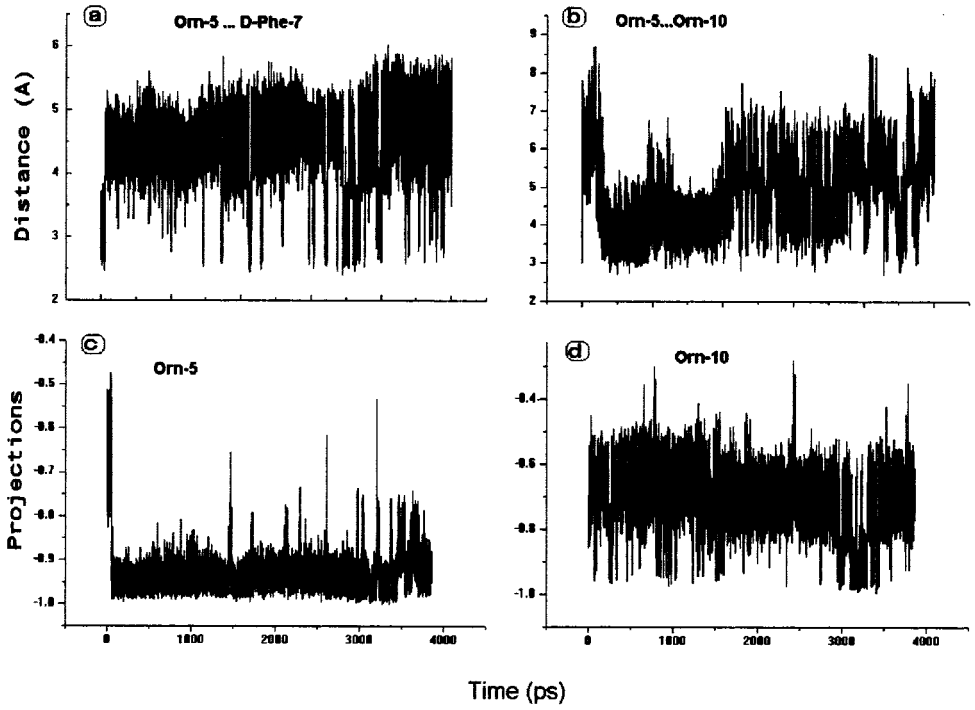

Figure 8. Time series of distance between the (a) N_δ atom of Orn-5 and O atom of D-Phe-7 and between (b) N_δ of Orn-5 and N_δ of Orn-10. (c, d) Main unitary vector projections in *z* direction for the Orn residues. The unitary vectors are defined from C_α to N_δ of the Orn each residue. The *z* direction is the direction of normal to the ellipical plane of the backbone of GS.

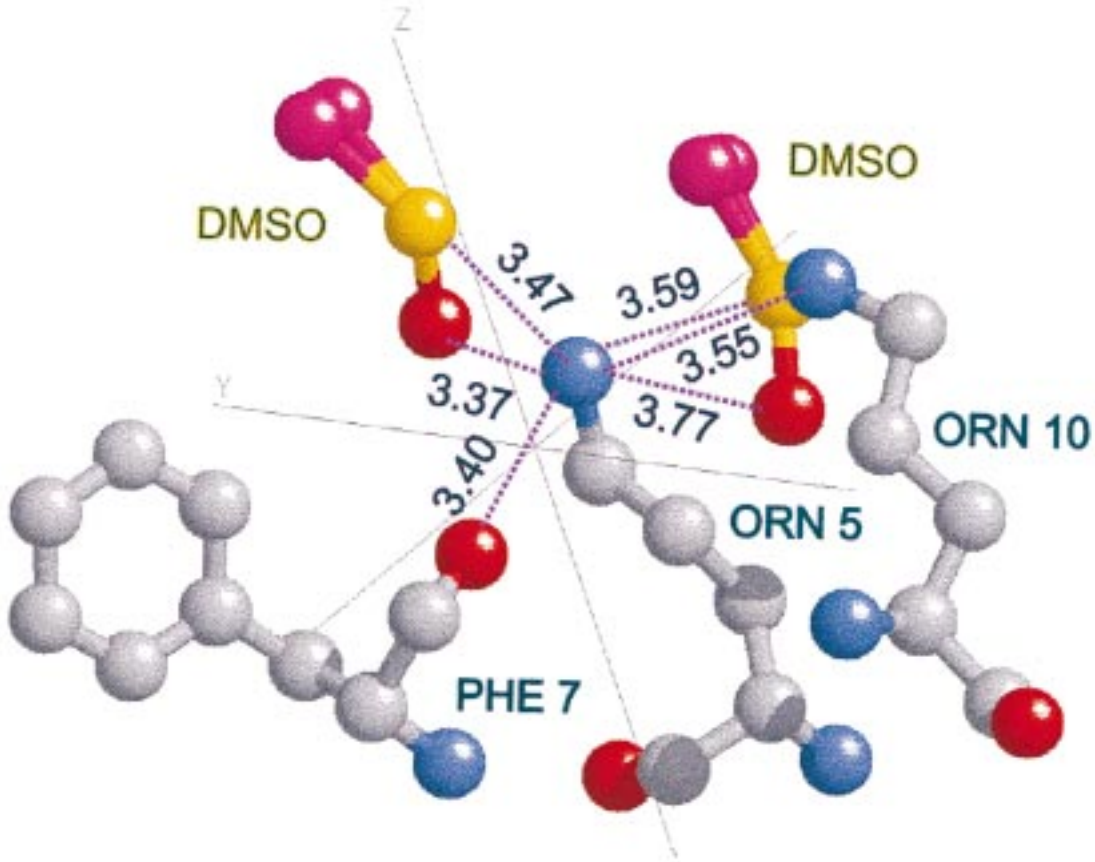

Figure 9. Relative positions of the two Orn residues, D-Phe-7, and the closest DMSO molecules around the N_δ atom of Orn-5. The methyl groups of DMSO are represented as single atoms. The plot was obtained using the "RASMOL" software.

interaction to permit the obtention of a useful starting structure for a membrane−GS simulation.[24] Work in this direction is in progress. A detailed simulation model of lipid−GS interactions should lead to direct practical applications and in particular might enable rules governing three-dimensional structure−activity relationships to be established. An end goal of this would thus be the rational use of simulation-derived conformational and energetic information in the design of GS derivatives of

comparable or enhanced antibiotic effects but with markedly diminished hemolytic activity.

Appendix

Topology and Parameter CHARMM Files for Ornithine and DMSO

```
RESI ORNN        0.00 ! Neutral Ornithine
GROU
 ATOM N    NP    -0.40
 ATOM HN   H      0.25
 ATOM CA   CT     0.05
 ATOM HA   HA     0.05
GROU
 ATOM CB   CT    -0.10
 ATOM HB1  HA     0.05
 ATOM HB2  HA     0.05
 ATOM CG   CT    -0.10
 ATOM HG1  HA     0.05
 ATOM HG2  HA     0.05
GROU
 ATOM CD   CT    -0.10
 ATOM HD1  HA     0.05
 ATOM HD2  HA     0.05
 ATOM NZ   NT    -0.30
 ATOM HZ1  H      0.15
 ATOM HZ2  H      0.15
GROU
 ATOM C    C      0.60
 ATOM O    O     -0.55
BOND  N HN   N CA   CA C   C O   C +N
BOND  CA HA   CA CB   CB HB1   CB HB2   CB CG   CG HG1   CG HG2
BOND  CG CD   CD HD1   CD HD2   CD NZ   NZ HZ1   NZ HZ2
IMPH  N -C CA HN   C CA +N O
DONO  HN N
DONO  HZ1 NZ
DONO  HZ2 NZ
ACCE  O C
IC    -C N CA C          0.00  0.00  180.00  0.00  0.00
IC    N CA C +N          0.00  0.00  180.00  0.00  0.00
IC    CA C +N +CA        0.00  0.00  180.00  0.00  0.00
IC    -C CA *N HN        0.00  0.00  180.00  0.00  0.00
IC    CA +N *C O         0.00  0.00  180.00  0.00  0.00
IC    N C *CA CB         0.00  0.00  120.00  0.00  0.00
IC    N C *CA HA         0.00  0.00  240.00  0.00  0.00
IC    N CA CB CG         0.00  0.00  180.00  0.00  0.00
IC    CG CA *CB HB1      0.00  0.00  120.00  0.00  0.00
IC    CG CA *CB HB2      0.00  0.00  240.00  0.00  0.00
IC    CA CB CG CD        0.00  0.00  180.00  0.00  0.00
IC    CD CB *CG HG1      0.00  0.00  120.00  0.00  0.00
IC    CD CB *CG HG2      0.00  0.00  240.00  0.00  0.00
IC    CB CG CD NZ        0.00  0.00  180.00  0.00  0.00
IC    NZ CG *CD HD1      0.00  0.00  120.00  0.00  0.00
IC    NZ CG *CD HD2      0.00  0.00  240.00  0.00  0.00
IC    CG CD NZ HZ1       0.00  0.00  180.00  0.00  0.00
IC    HZ1 CD *NZ HZ2     0.00  0.00  120.00  0.00  0.00
```

```
RESI dmso          0.000
GROUP
ATOM M1 M          0.160
ATOM M2 M          0.160
ATOM S3 SD         0.139
ATOM O4 OD        -0.459
BOND M1 S3
BOND M2 S3
BOND S3 O4
ACCEPTOR O4
```

```
MASS   204  M      15.0350
MASS   205 OD      15.9994
MASS   206 SD      32.0600
```

```
!              EMIN        Rmin
!              (kcal/mol)    (A)

OD             -0.4100      1.315
M              -0.2250      1.830
SD             -0.3100      1.780

Bonds

OD  SD        999.9       1.53
M   SD        999.9       1.95

Thetas

M   SD  M     99.9       97.4
M   SD  OD    99.9      106.75
```

References and Notes

(1) Gause, G. F.; Brazhnikova, M. G. *Nature (London)* **1944**, *154*, 703.

(2) Kondejewski, L. H.; Farmer, S. W.; Wishart, D. S.; Hancock, R. E.; Hodges, R. S. *Int. J. Pept. Protein Res.* **1996**, *47*, 460.

(3) Katsu, T.; Ninomiya, C.; Kuroko, M.; Kobayashi, H.; Hirota, T.; Fujita, Y. *Biochim. Biophys. Acta* **1988**, *939*, 57.

(4) Katsu, T.; Kobayashi, H.; Fujita, Y. *Biochim. Biophys. Acta* **1986**, *860*, 608.

(5) Portlock, S.;H.; Clague, M. J.; Cherry, R. J. *Biochim. Biophys. Acta* **1990**, *1030*, 1.

(6) Goodall, M. C. *Biochim. Biophys. Acta* **1970**, *219*, 471.

(7) Ovchinnikov, Y. A.; Ivanov, T. *Tetrehedron* **1975**, *31*, 2177.

(8) Datema, K. P.; Pauls, K. P.; Bloom, M. *Biochemistry* **1986**, *25*, 3796.

(9) Zidovetzki, R.; Banerjee, U.; Harrigton, D. W.; Chan, S. I. *Biochemistry* **1988**, *27*, 5686.

(10) Prenner, E. J.; Lewis, R. N. A. H.; Neuman, K. C.; Gruner, S. M.; Kondejewski, L. H.; Hodges, R. S.; McElhaney, R. N. *Biochemistry* **1997**, *37*, 7906.

(11) Hull, E.; Karlsson, R.; Main, P.; Woolfson, M. M.; Dodson, E. J. *Nature* **1978**, *75*, 206.

(12) Stern, A.; Gibbons, W. A.; Craig, L. C. *Proc. Natl. Acad. Sci.* **1968**, *61*, 734.

(13) Jones, C. R.; Sikakana, C. T.; Hehir, S.; Kuo, M.-C.; Gibbons, W. A. *Biophys J.* **1978**, *24*, 815.

(14) Esposito, G.; Pastore, A. *J. Magn. Res.* **1988**, *76*, 331.

(15) Kuo, M.-C.; Jones, C. R.; Mahn, T. H.; Miller, P. R.; Nicholls, L. J. F.; Gibbon, W. A. *J. Biol. Chem.* **1979**, *254*, 10301.

(16) Gondol, D.; Van Binst, G. *Biopolymers* **1986**, *25*, 977.

(17) Rae, I. D.; Scheraga, H. A. *Biochem. Biophys. Res. Commun.* **1978**, *81*, 481.

(18) Krauss, E. M.; Chan, S. I. *J. Am. Chem. Soc.* **1982**, *104*, 6953.

(19) Jones, C. R.; Kuo, M.-C.; Gibbons, W. A. *J. Biol. Chem.* **1979**, *254*, 10307.

(20) Xu, Y.; Sugar, I. P.; Krishna, N. R. *J. Biomol. NMR* **1995**, *5*, 37.

(21) Abbott, N. B.; Ambrose, E. J. *Proc. R. Soc., Ser. A* **1953**, *219*, 17.

(22) Kamegai, J.; Kimura, S.; Imanishi, Y. *Biophys. J.* **1986**, *49*, 1101.

(23) Craig, L. C. *Proc. Natl. Acad. Sci.* **1968**, *61*, 152.

(24) Tetsuo, K.; Izumiya, N. *Biochim. Biophys. Acta* **1977**, *493*, 235.

(25) Yagi, Y.; Kimura, S.; Imanishi, Y. *Int. J. Pept. Prot. Res.* **1990**, *36*, 18.

(26) Tamaki, M.; Akabori, S.; Muramatsu, I. *Int. J. Pept. Protein Res.* **1996**, *47*, 369.

(27) Ando, S.; Nishihama, M.; Nishikawa, H.; Takiguchi, H.; Lee, S. *Int. J. Pept. Protein Res.* **1995**, *46*, 97.

(28) Hodgkin, D. C.; Oughton, B. M. *Biochemistry* **1957**, *65*, 752.

(29) Rackovsky, S.; Scheraga, H. A. *Proc. Natl. Acad. Sci. U.S.A.* **1980**, *77*, 6965.

(30) Dygert, M.; Go, N.; Scheraga, H. A. *Macromolecules* **1975**, *8*, 750.

(31) Momany, F. A.; Vanderkooi, G.; Tuttle, R. W.; Scheraga, H. A. *Biochemistry* **1969**, *8*, 744.

(32) Nemethy, G.; Scheraga, H. A. *Biochem. Biophys. Res. Commun.* **1984**, *118*, 643.

(33) Brooks, B. R.; Bruccoleri, R. E.; Olafson, B. D.; States, D. J.; Swaminathan, S.; Karplus, M. *J. Comput. Chem.* **1983**, *4*, 187.

(34) MacKerell, A. D., Jr.; Bashford, D.; Bellot, M.; Dunbrack, R. L., Jr.; Evanseck, J. D.; Filed, M. J.; Ficher, S.; Gao, J.; Guo, H.; Ha, S.; Joseph-McCarthy, D.; Kuchnir, L.; Kuczera, K.; Lau, F. T. K.; Matos, C.; Michnick, S.; Ngo, T.; Nguyen, D. T.; Prodhom, B.; Reiher, W. E.; Roux, B.; Schlenkrich, M.; Smith, J. C.; Stote, R.; Straub, J.; Watanabe, M.; Wiorkiewicz-Kuczere, J.; Yin, D.; Karplus, M. *J. Phys. Chem. B* **1998**, *102*, 3586.

(35) Liu, H.; Müller-Plathe, F.; van Gunsteren, W. F. *J. Am. Chem. Soc.* **1995**, *117*, 4363.

(36) van der Spoel, D.; Berendsen, H. J. C. *Biophys. J.* **1997**, *72*, 2032.

(37) Levitt, M. *J. Mol. Biol.* **1983**, *168*, 621.

(38) Karpen, M.; Tobias J. D.; Brooks, L. C., III. *Biochemistry* **1993**, *32*, 412.

(39) Balasubramanian, D. *J. Am. Chem. Soc.* **1967**, *89*, 5445.